Materials & Design 226 (2023) 111601

Contents lists available at ScienceDirect

Materials & Design

journal homepage: www.elsevier.com/locate/matdes

Multi-scale modelling of the mechanical behaviour of a CoNiCrAlY bond coat alloy during small punch testing

K. Sithole [a], C.L. Taylor [a], J.P. Rouse [a], C.J. Hyde [a,*]

[a] Department of Mechanical, Materials, and Manufacturing Engineering, University of Nottingham, Nottingham, Nottinghamshire NG7 2RD, UK

HIGHLIGHTS

- 2D representative volume elements of CoNiCrAlY are generated and the effective Young's modulus and Poisson's ratio are validated with analytical expressions.
- The impact of volume fraction of the beta-phase part of CoNiCrAlY on its Young's modulus and Poisson's ratio is studied.
- The force–displacement response of a finite element model of the small punch tensile test is compared with the response from representative volume elements.
- The small punch tensile test is found to be insensitive to changes in the volume fraction of the CoNiCrAlY.

GRAPHICAL ABSTRACT

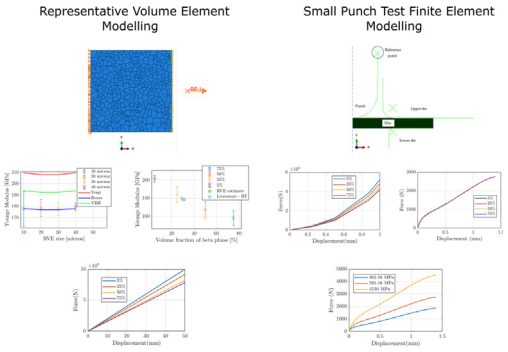

ARTICLE INFO

Article history:
Received 27 September 2022
Revised 3 January 2023
Accepted 5 January 2023
Available online 16 January 2023

Keywords:
Representative volume element
CoNiCrAlY
Bond Coats
Small punch test
Finite element modelling

ABSTRACT

The present work is undertaken to determine the ability of the small punch test to determine mechanical properties of CoNiCrAlY, a two phase bond-coat material found in thermal barrier coatings. It utilises a multi-scale modelling methodology in which 2-dimensional representative volume elements of CoNiCrAlY and finite element models of the small punch test are developed. Effective Young's moduli and Poisson's ratios are obtained from the representative volume elements and are compared with those obtained from analytical homogenization through the Voigt, Reuss and Voigt-Reuss-Hill schemes. The volume fraction of the β-Nial phase in CoNiCrAlY is varied and the force–displacement responses of representative volume elements are contrasted with those from small punch test finite element models, through comparison of ratios of discrete fréchet distances. The results of the study estimated Young's modulus and Poisson's ratio to be 178.56 ± 7.65GPa and 0.249 ± 0.037 respectively, and for an increasing β-Nial phase volume fraction, the Young's modulus and Poisson's ratio decrease. Lastly, the results suggest that the small punch test is insensitive to variations in material elastic behaviour because its results are more influenced by the yield properties of a material.

1. Introduction

The demand for more efficient aircraft and power plant requires components to operate at increasingly high temperatures. However, designing hotter systems brings about challenges due to the

* Corresponding author.

https://doi.org/10.1016/j.matdes.2023.111601
0264-1275/

increased degradation of materials in such environments. Components such as turbine blades are exposed to gases with high temperatures that can ex 1650 °C [1]. These temperatures exceed the melting points of materials such as Ni superalloys, that are used to make the turbine blades and which typically have a melting point of 1300 °C[2]. As a result, degradation mechanisms such as corrosion, thermal fatigue, creep and oxidation are prevalent [1–3]. This can result in premature failure of components incurring significant material, time and financial costs.

Evaluating the material properties of structural components is a crucial part of conducting life assessments. When a limited amount of material is available, small- scale specimen testing procedures like the Small Punch Test (SPT) have availed as appropriate testing solutions. The SPT is a widely used experimental procedure used for testing specimens that are of a small scale, with typical thicknesses of 0.2–0.5 mm [4–7]. The sample specimen can be obtained from scoop sampling of in-service power plant components or in other applications such as blade root, a blade is removed and destroyed to obtain samples. An example of an industrial material that undergoes small punch testing is thermal barrier coatings (TBCs). TBCs are multilayer system deposited on the surface of turbine blades to protect them from the harsh environments in the engine. They consist of a superalloy substrate, a metallic alloy bond coat and ceramic top coat [8]. In small-scale methodologies, the nature of the specimen or test type makes data interpretation difficult. This is due to the shape of the specimen being frequently non-linear for example and in addition, it is not reasonable to assume that all material deformation modes are equivalently captured by the small specimen approach. Finite Element Analysis (FEA), has been employed to model the SPT in creep applications and the measurement of ductile to brittle transition temperatures [6,9,10]. However, in literature there has not yet been a study undertaken to determine the sensitivity of the test's results, to variations in the constituents of the material tested. A study like this will determine whether a change in underlying material constitutive properties consequently results in a correlated change in the output of the SPT. The significance of this lies in the challenge of quantification of uncertainty in the mechanical response measured through the SPT. This is due to the uncertainties present in the various ways the SPT is set-up and conducted and, for materials like CoNiCrAlY uncertainties that come about due to the different spraying techniques implemented in its manufacture.

Accordingly, the current work will determine the ability of the SPT in measuring mechanical properties of CoNiCrAlY, a two phase bond coat material found in TBCs. This is done by first evaluating the sensitivity of the Young's modulus and Poisson's ratio of CoNiCrAlY to changes in volume fraction of one of its constituent phases. Subsequently an evaluation of the sensitivity of the Young's modulus and Poisson's ratio of CoNiCrAlY from a SPT computational model is presented. The results from the two sensitivity analyses are contrasted to determine whether the elasto-plastic SPT response is sensitive to changes in the underlying material properties of CoNiCrAlY or if they are more impacted by other factors. In this case, TBCs are particularly relevant to small punch testing because of their small thicknesses (~100 μm) in service, which require small-scale testing procedures.

1.1. Small punch test

The SPT originated in the US and Japan in the 1980 s [6]. Its advantage stems from its ability to derive standard material properties when very limited amounts of material are available [11,12]. Fig. 1 shows a schematic of the typical test set up. The test constitutes of the punch which is pushed through a specimen disc clamped by the upper and lower die. The resulting deflection of either the punch or the specimen is measured along with the required force to drive the punch. The test can be conducted at constant displacement rate of the punch (akin to a uniaxial stress–strain test [13]) or at constant force which results in a creep test. Mechanical properties like Young's mod- ulus and Poisson's ratio (v) can then be derived from the results. However, because of the triaxial nature of the test due to the inherent additional bending of the disc, and the sensitivity of the test results to specimen geometry, obtaining measurements directly from the test is a challenge [12]. At present, there exists no universally accepted stand- ard for SPT operation. However, prominent international standards do exist which are BS EN 10371:2021, ASTM E3205 20 and GB/T 29,459 which are contributions from Europe, America, and China. These standards provide guidelines for determining elastic–plastic transition, ductile–brittle transitions, and failure properties. But there exists a large scatter between results from different testing facilities which arises due to the experimental setup [14]. The European standard which is referenced the most in the literature makes allowances for the choice of position for the measurement of the deflection of the specimen, allowing for the measurement to be made locally (underneath the specimen) or remotely from the cross-head, which has been shown to cause significant differences in SPT response and compliance errors. Additionally, compliance corrections due to the stiffness of the punch and geometry of the dies along with test misalignment issues can affect the results of the test [15,16]. These issues that have been stated highlight the significance of performing the current study.

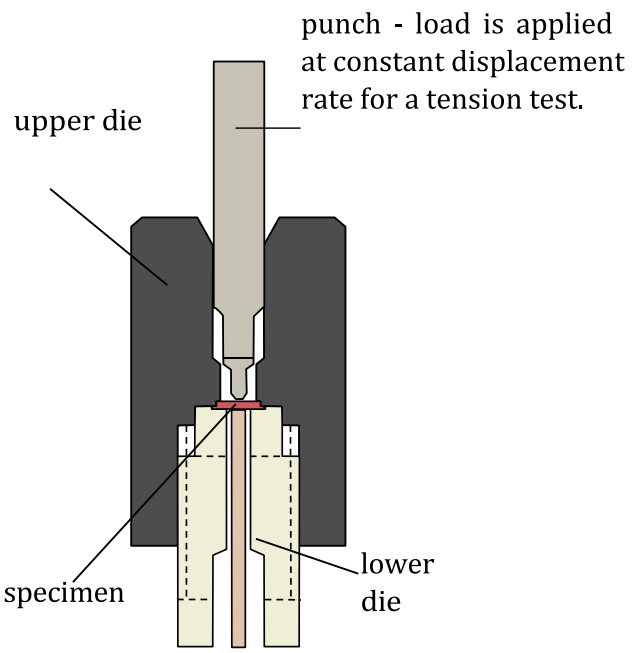

Fig. 1. A typical Small Punch Test Experimental set up [6].

Literature presents two different relationships for the expected force–displacement curves of SPT results. Fig. 2a represents the expected force–displacement relationship for a SPT of a ductile failure. It consists of distinct regions widely accepted in literature [17–19] namely: (1) elastic region (2) yielding (3) plastic bending (4) membrane stress regime (5) final failure region. Fig. 2b however, shows the expected force- displacement results for a brittle failure. The brittle failure presents a much more dominant linear region with sharp drops in load throughout testing [5], with the force drops indicating crack initiation [20].

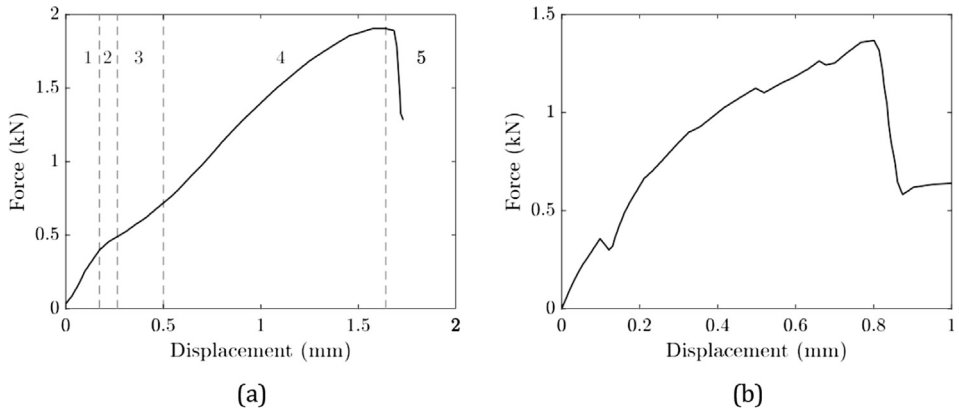

Fig. 2. Diagrams showing the force–displacement curves of (a) a ductile material and (b) a brittle material.

1.2. CoNiCrAlY Bond-Coat

CoNiCrAlY is a complex, multi-phase polycrystalline material that consists of face- centred cubic (fcc) γ-Ni and body-centred cubic (bcc) β-NiAl phases [21]. It is extensively used as a material in bond-coats in TBC systems which are responsible for providing thermal insulation to components such as turbine blades against high temperature gases. To combat premature failure, TBCs coupled with active cooling are employed to reduce the temperature effects on turbine blades [8], for example. Fig. 3 is a diagram of a turbine blade with the TBC system employed.

Together with active cooling (a process of blowing cool air through the inner surface of the turbine blade) TBCs have been shown to reduce blade temperature by as much as 139 °C [1]. However, due to thermal-expansion mismatch between the bond-coat and the top-coat as well as the change in properties of bond-coats during in-service, result in spallation of the bond-coat and its premature failure hence compromising the whole TBC system. Accordingly, the failure of the bond-coat dictates the failure of the system and hence the turbine blade [8]. This investigation will determine the limitations that impact the measurement of mechanical properties of the bond-coat which will consequently inform the behaviour of TBCs.

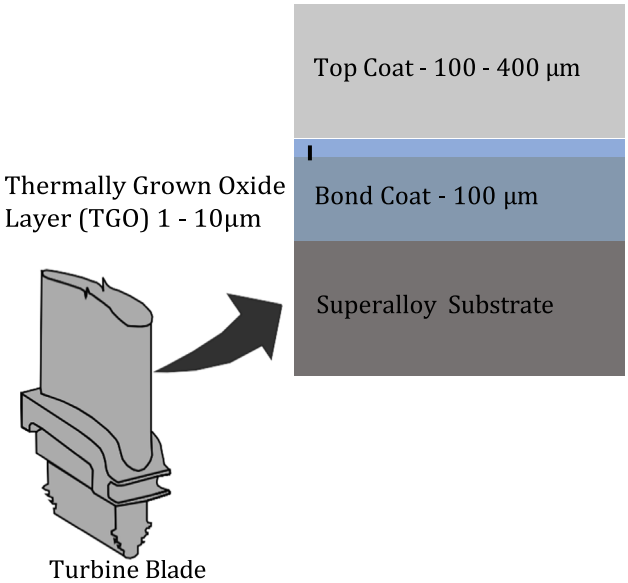

Fig. 3. TBC system on a turbine blade [8].

Fig. 4a and 4b show diagrams obtained from Electron Backscatter Diffraction (EBSD). Fig. 4a shows an electron micrograph of CoNiCrAlY at a microscopic scale. The diagram shows the different phases of the material (dark grey phases represent β-NiAl, lighter phases are γ-Ni and black regions are voids). Fig. 4b shows an inverse pole diagram illustrating the different grain orientations in the polycrystalline material. In its application in TBCs, the thickness of CoNiCrAlY is approximately 100 µm. At this dimension the bond-coat thickness has a length scale that is comparable to the size of its individual grains. Therefore, determining the overall mechanical behaviour of the component must factor in the influence of the location and orientation of grains. In this study, overall mechanical behaviour is determined by varying the distribution of the γ-Ni and β-NiAl phase as well as the orientations of grains. Focus is given to the elastic behaviour of CoNiCrAlY as the debonding that occurs of the bond-coat in TBCs is predominantly driven by the presence of residual stresses. When residual stresses are 'relaxed' this results in a release of stored elastic strain energy which controls the propagation of interfacial cracks between the bond-coat and the substrate [22]. Hence, the Young's modulus is an important quantity and is determined in this study along with the Poisson's ratio. To define the elastic behaviour of the material, single crystal elastic constants are assigned to the two types of cubic crystals that make up the two phases of CoNiCrAlY. Only three independent elastic constants are needed for each elastic stiffness matrix of the crystals that make up the two phases [23]. These constants are c_{11}, c_{12} and c_{44} positions in the elasticity matrices. These parameters are varied along with the distribution of the two phases and orientation of the grains to ensure that anisotropic properties of the material are accounted for in the overall response.

1.3. Multiscale modelling

At large length scales (macro-scale) a material like CoNiCrAlY is assumed to be homogeneous and isotropic however, in applications like in TBC bond-coats where the material's thickness is 100 µm, the anisotropic and heterogeneous properties of its micro-structure must be taken into account. Toonder et al [23] conducted a study to determine Young's modulus and Poisson's ratio of the polycrystalline material BaTiO3 in its application as a ceramic capacitor, and showed that due to the capacitor being only approximately 10 µm in thickness, the anisotropic properties of its individual grains must be accounted for. This is due to the thickness having a dimension that is within the same order of magnitude as the size of the grains making up the mater- ial. Consequently determining the effective Young's modulus and Poisson's ratio of BaTiO3 involved using micromechanics approaches namely: analytical averaging of single crystal anisotropy and finite

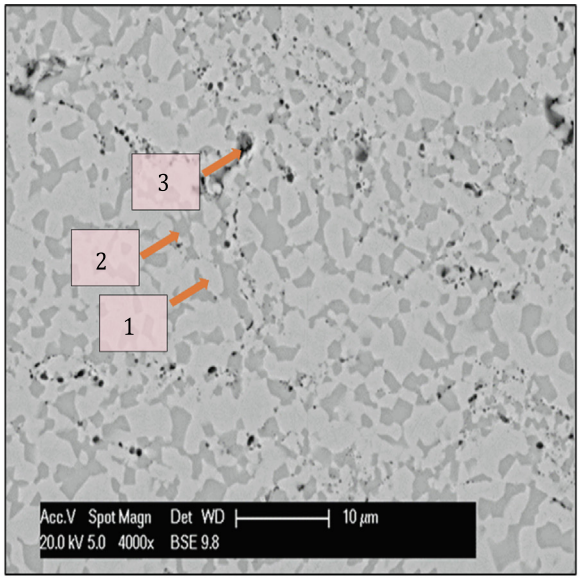

(a)

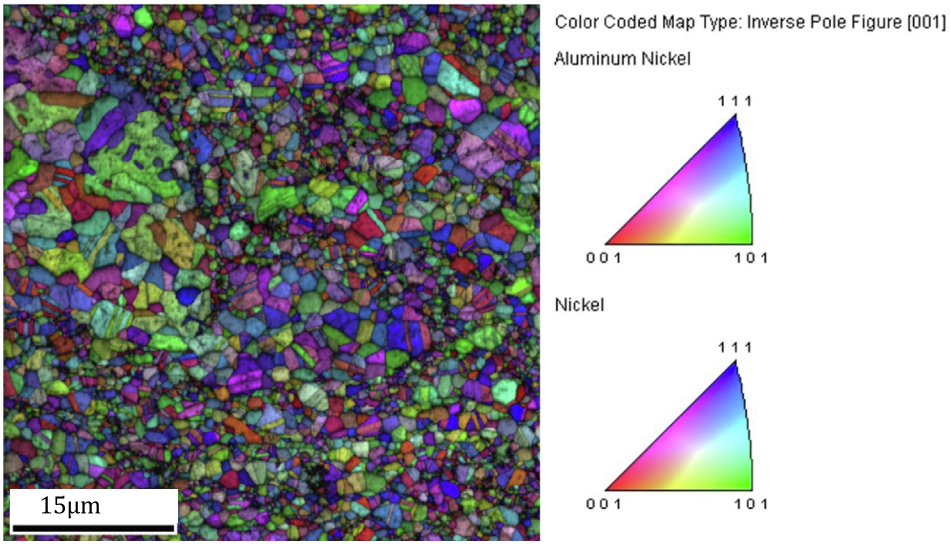

(b)

Fig. 4. Diagrams showing (a) phases present in CoNiCrAlY; (1) γ-Ni, (2) β-NiAl and (3) voids, (b) an inverse pole diagram with colours showing different grain orientations.

element modelling of small volumes of BaTiO3. However, in the present study a multiscale modelling procedure involving multiple modelling approaches at different length scales is employed. The procedure determines the effective elastic response of CoNiCrAlY at the micro and macro length scales by using: Voigt, Reuss and Voigt-Reuss-Hill (VRH) averaging methods (which are analytical methods used to determine effective Young's modulus and Poisson's ratio from single crystal anisotropy [23]); finite element modelling using representative volume elements (RVEs); and FE modelling of the SPT. The results of each of these approaches are used in conjunction with each other to determine the sensitivity of the SPT mechanical response to changes in the microstructure of CoNiCrAlY through the comparison of ratio of discrete fréchet distances. Fréchet distance is a measure of the similarity between two curves or lines on a plot and its implementation is in this study is discussed later in section 3.3.

2. Methodology

2.1. Material

Previous work was conducted by Jackson [24] focusing on the impact of microstructure on the mechanical response of CoNiCrAlY, which involved preparation of specimens of the material and characterisation. The current work uses the previously prepared material specimens in its investigation. The material was prepared using Praxair CoNiCrAlY powder (CO-210–24), which had a composition of Co-32.6 Ni-21.1 Cr-8.7 Al-0.43 (wt%) and was thermally sprayed on a steel substrate using High Velocity Oxygen Fuel (HVOF) method. The material was debonded from the substrate and vacuum heat treated at 1100 °C for 2 h, allowing the secondary β-phase to precipitate and reducing the porosity in the material. The resulting volume fraction of the material was determined to be 31 % β-phase, 68 % γ-phase while the remaining 1.4 % was attributed to the formation of an oxide (Al2O3) and

pores. EBSD was used to produce inverse pole figures to determine crystal orientations (see Fig. 4b) while Back Scatter Electron (BSE) images were used to determine the volume fraction of the phases (see Fig. 4a).

2.2. Finite element modelling of representative volume elements of CoNiCrAlY

To determine the effective elastic behaviour of CoNiCrAlY from its elastic constants, the method of RVEs was employed. An RVE is a computational volume of material that through a homogenization procedure allows the effective behaviour of the bulk material to be determined [25]. Generating RVEs for the study entailed understanding the material's microstructure, more specifically the distribution of its constituent β- phase and γ-phase, the orientations of its grains, their size and shape distribution [26]. Image analysis using MATLAB was conducted to convert BSE images into greyscale, in order to intensify the contrast between the darker grey β-NiAl phase and the lighter grey γ-Ni phase to convert the image into binary. Properties relating to the shape, area and distribution of the phases are extracted and are used in the construction of RVEs. Subsequently, Voronoi tessellation was employed to discretize the geometry of the RVE. This was also done through MATLAB by using sets of points on the RVE and creating cells from these points, with the cell boundaries equidistant from the points used to generate the cells. This can be seen in Fig. 5a, where the cell boundaries of the Voronoi elements represent the grain boundaries. Material elastic constants and grain orientations are added to the RVE to define the material properties (see Fig. 5b). This allocation of material properties to the Voronoi elements which represent the grains in the material, depends on the morphology determined from the BSE and EBSD. Therefore, in the RVE some Voronoi cells are assigned to β-NiAl phase while the rest are assigned to γ-Ni phase. Fig. 6 shows the series of steps taken to develop the RVE FE models to determine the effective Young's modulus and Poisson's ratio of CoNiCrAlY. After generating RVEs in step 1 in the diagram, MATLAB scripts obtain elastic constants of the Ni and NiAl phase. The NiAl material constants obtained from [27] are provided with a mean and standard deviation as seen from Table 1. Latin Hypercube Sampling (LHS) was used to obtain 30 samples from the NiAl confidence intervals in Table 1 whilst the Ni phase constants remained the same. The 30 samples taken correllate to 30 RVEs, one for each NiAl phase sample. The advantage of LHS is that it obtains samples both uniformly and randomly in the sample space, which reduces the amount of samples needed whilst maintaining a good level of spread in the sampled data [28]. In Step 3 in Fig. 6, Abaqus FE software is used to apply boundary and load conditions to the RVE and create input files for computational solutions. In Fig. 5a, an RVE is shown with the boundary conditions applied. The left edge of the RVE shows boundary conditions (orange triangles) which are placed to prevent movement in the x-direction while allowing translation in the y-direction. The boundary conditions placed on the bottom edge on the left corner accounts for rigid body motion. On the right edge, an equation constraint is placed relating the displacement of the right edge to the reference point (RP). A load condition is applied to the RP defining a horizontal translation. and thereby applying tension to the RVE. These steps are repeated by applying the load and boundary conditions accordingly to produce tension in the RVE in the y-direction, where the boundary conditions that prevent motion are placed on the bottom edge of the RVE and an equation constrain is placed between the top edge and another reference point adjacent to the top edge. Resultant forces from the reference points along with the resulting displacements obtained from the edges, are used to calculate stresses and strains from which Young's modulus and

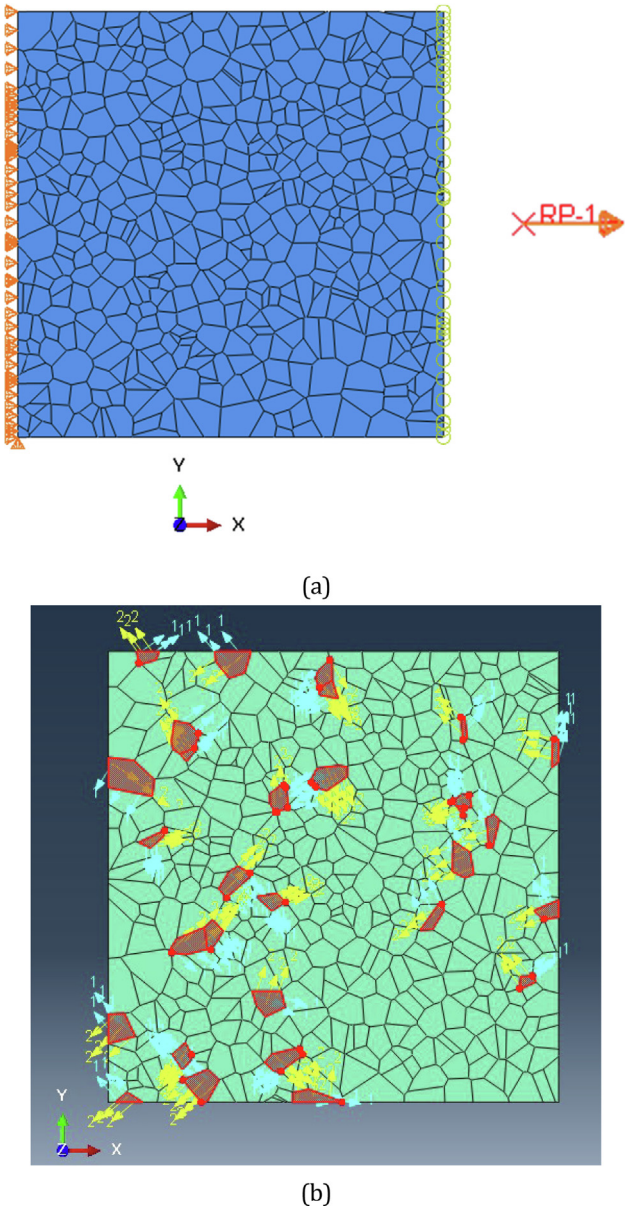

Fig. 5. Illustrations showing (a) RVE with boundary conditions (shown as orange triangles) and equation constraints (shown as yellow circles) connected to a reference point (shown as RP-1). The boundary conditions prevent translation in the x-direction and rigid body motion in the y-direction. And (b) RVE showing random orientations applied to voronoi cells (in this case only a few cells are selected). (For interpretation of the references to colour in this figure legend, the reader is referred to the web version of this article.)

Poisson's ratio are calculated and are compared with results from analytical methods.

Fundamental to the method of RVE and homogenization is the determination of an appropriate size of the RVE. The methodology shown in Fig. 6 was used to investigate the appropriate size of RVE by determining effective Young's modulus and Poisson's ratio from varying the size of the RVE. The results obtained from the FE model were compared to results from Voigt, Reuss, VRH analytical homogenization methods for effective Young's modulus and Poisson's ratio of the bulk material. These analytical methods have been used in previous studies [25,29] to give indications of effective elastic properties from single crystal elasticity and in this study they are used as comparison with effective properties derived from RVE numerical homogeniza- tion and those obtained

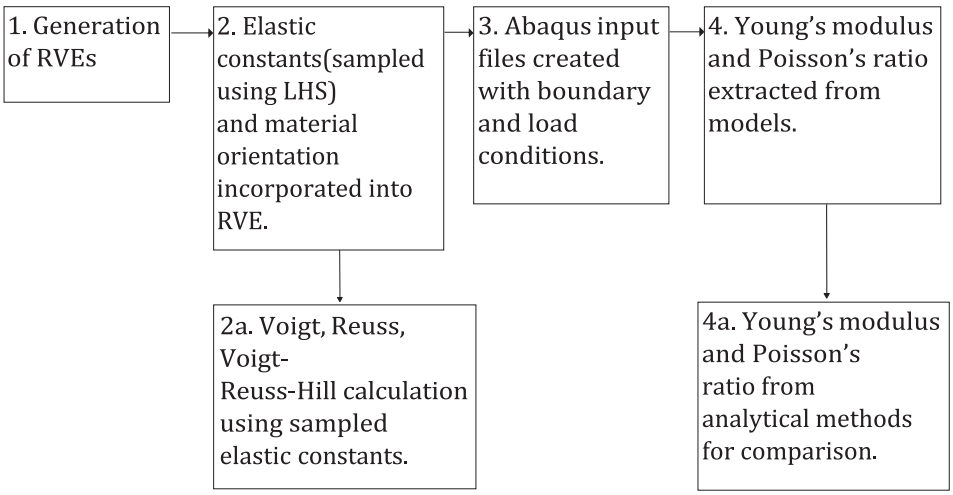

Fig. 6. Process taken in generating RVEs, numerical testing and extracting mechan- ical properties.

Table 1
Values shown are the mean and standard deviation of β-NiAl and γ-Ni phase elastic constants [27].

	c_{11}[GPa]	c_{12}[GPa]	c_{44}[GPa]
NiAl	198 ± 5	137 ± 3	116 ± 3
Ni	286.9	128.9	79

from literature (see Fig. 8a and 11a). The Voigt scheme is derived from averaging the fourth-order elasticity tensor of crystals in all feasible orientations, whilst the Reuss scheme averages the compliance tensor instead, which is the inverse of the elasticity tensor. The VRH scheme however, gives the mean of the two schemes. Hence, the Voigt and Reuss techniques give the upper and lower bounds of the effective Young's modulus and Poisson's ratio while the VRH gives values that lie midway between the two bounds. Toonder et al [23] details how these techniques can be implemented, this is explained in the following paragraphs.

Equations 1 and 2 show how the Voigt homogenization was conducted to determine Young's modulus E_v and Poisson's ratio υ_v. The values for $c11$ to $c66$ represent elastic constants of an elasticity matrix, however because both phases of CoNiCrAlY are cubic crystals, only three independent elastic constants are needed to define the elasticity matrix and these constants are shown in Table 1. Therefore, in equation 2 the following is true: $c_{22} = c_{33} = c_{11}$, $c_{23} = c_{13} = c_{12}$ and $c_{55} = c_{66} = c_{44}$. Equations 3 and 4 however, show how the Reuss averaging was conducted. In this case s_{11} to s_{66} are the values in the compliance tensor but due to the cubic nature of the phases, the following is true: $s_{22} = s_{33} = s_{11}$, $s_{23} = s_{13} = s_{12}$ and $s_{55} = s_{66} = s_{44}$. Finally, equations 5 shows the VRH calculation which is the mean of the two averaging schemes.

$$E_V = \frac{(\alpha - \beta + 3\gamma)(\alpha + 2\beta)}{2\alpha + 3\beta + \gamma} \quad \upsilon_v = \frac{(\alpha + 4\beta - 2\gamma)}{4\alpha + 6\beta + 2\gamma} \tag{1}$$

$$\alpha = \frac{(c_{11} + c_{22} + c_{33})}{3} \quad \beta = \frac{(c_{23} + c_{13} + c_{12})}{3} \quad \gamma = \frac{(c_{44} + c_{55} + c_{66})}{3} \tag{2}$$

$$E_R = \frac{5}{3\alpha' + 2\beta'\gamma'} \quad \upsilon_R = -\frac{2\alpha' + 8\beta' - \gamma'}{6\alpha' + 4\beta' + 2\gamma'} \tag{3}$$

$$\alpha' = \frac{(s_{11} + s_{22} + s_{33})}{3} \quad \beta' = \frac{(s_{23} + s_{13} + s_{12})}{3} \quad \gamma' = \frac{(s_{44} + s_{55} + s_{66})}{3} \tag{4}$$

$$E_{VRH} = \frac{1}{2}[E_V + E_R] \quad \upsilon_{VRH} = \frac{1}{2}[\upsilon_V + \upsilon_R] \tag{5}$$

2.3. Finite element modelling of the small punch test

The primary purpose of this research is to investigate the SPT's ability in measuring mechanical properties by studying the sensitivity of its force–displacement results to changes in β phase volume fraction of CoNiCrAlY, which is the test material. Therefore, an FE model of the test has been created and simulated with effective Young's moduli and Poisson's ratio obtained from RVE estimates of different volume fractions of β phase, measured from the previous RVE study. A correlated change in steepness of the elastic zone (of the SPT model force–displacement results) with variation in material parameters, will show the test's sensitivity to changes in specimen material parameters. In the model setup

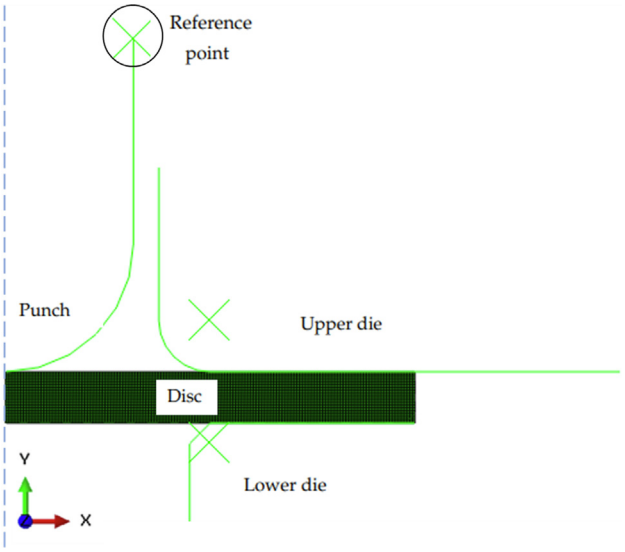

Fig. 7. FE Small Punch Test Model.

Abaqus FE software was employed to create an axisymmetric model of the SPT shown in Fig. 7. The elements used in the model were CAX4H 4-node bilinear axisymmetric quadrilateral elements. In Fig. 7, the punch is driven through the clamped disc made of CoNiCrAlY. The displacement and resultant force of the punch is measured from the reference point located on the punch. Table 2 shows the geometry of the features in the model which are representive of actual experimental setups and other FE models in literature [6–10]. In addition, plastic material properties of CoNiCrAlY were added to the FE SPT model to better approximate the response of the test. This was done by applying Johnson-Cook constitutive properties obtained from Wen [20] shown in Table 3, where parameters A, B, n and m represent the yield stress, strain hardening coefficient, strain hardening exponent and the material constant for thermal softening exponent, respectively [20].

3. Results

3.1. Results from the FE modelling of RVES of CoNiCrAlY

Fig. 8a and 8b show the mean and standard deviation of effective Young's modulus and Poisson's ratio with an increasing size of RVE. As can be seen from the diagrams, the spread of the results decreases as the RVE size increases. This is an expected result as an increase in size of RVE results in more grains present in the material, which consequently results in a better average of effective response. However, as the size of RVE is increased, the computation cost increases. From Fig. 8b the effective poisson's ratio values show a similar trend of decreasing spread with increasing RVE size.

An RVE of 20 μm was chosen to be used in the next stages of analysis because it provided a reasonable computation time. Furthermore, to validate whether the RVE 20 μm could be considered isotropic and homogenized, the effective Young's modulus and Poisson's ratio in the × and y loading directions are compared. It can be seen from Fig. 9a and 9b that mean values of both properties in both loading directions (here load direction-11 refers to the × direction while load direction-22 refers to the y direction) have very similar values with each result lying within 1.5 % of each other. The spread in the results between loading directions for each parameter is comparable with significant overlap. This indicates that the RVE size is adequate enough to assume that the RVE has been homogenized.

Fig. 10 shows a diagram illustrating the β-NiAl grains with increasing volume fraction of β-phase. The volume fractions modelled are 5 %, 25 %, 50 % and 75 % which were arbitrarily chosen to highlight the impact of volume fraction of the β-phase on the effective response. The volume fractions from Fig. 10 were used in RVE models to obtain the effective responses. The results can be seen in Fig. 11a and 11b, which show a decreasing effective response for both Young's modulus and Poisson's ratio for increasing β-phase volume fraction. In addition, in Fig. 11a the results from the previous RVE study (for 40 μm RVE size) are plotted against values from a study conducted by Saeidi et al [30] where their material was also processed through HVOF, annealed at the same conditions of the material in this study and tested via Three Point Bending tests at room temperature. The material from Saeidi's study had a volume fraction of 30 % β-phase which is very similar to 31 % β-phase which is the volume fraction of the material used in the current study.

Table 2
Dimensions of FE Small Punch model.

Feature	Size
Punch diameter	2 mm
Plate diameter	8 mm
Plate thickness	0.5 mm
Chamfer dimensions (lower die)	0.2mmx45°
Diameter of receiving hole	4 mm

Table 3
Johnson-Cook constitutive properties at room temperature[20].

Parameter	Value
A	765.15 MPa
B	607.18
n	0.3
m	1.715

3.2. Results from FE modelling of the small punch test

Fig. 12b shows a plot of force–displacement from FE SPT simulations for different volume fractions of β-phase for conditions where elastic behaviour is solely considered. It can be seen that for an increasing volume fraction of β-phase, the steepness of the response reduces. Fig. 13a illustrates the response when material yield and hardening is implemented in the simulations. The force–displacement response here at each volume fraction falls on top each other such that there are negligible differences in the response.

In addition, Fig. 13b presents the response in the SPT model results when the yield stress is varied. Here the yield stress is halved and subsequently doubled. Similarly, in Fig. 12a showing force–displacement response for RVEs at different volume fractions, the same trend of decreasing steepness in the response is observed.

3.3. Results from sensitivity study using Fréchet distances

To determine the sensitivity of the SPT, it was important to establish whether changes in the properties of the CoNiCrAlY specimen material resulted in a corresponding proportional change in the force–displacement response of the test. Thus the response of the RVE (which is the material of the specimen in the SPT) in Fig. 12a is compared with the response of the SPT for the elastic case (see Fig. 12b) and the case with yield and hardening implemented (see Fig. 13a). The diagrams mentioned here illustrate the force–displacement plots for changing β-phase volume fraction. Comparison was made by first calculating discrete fréchet distances between different lines of volume fraction in Fig. 12a, determining the ratio of fréchet distances between the lines and comparing this ratio with those ratios obtained from Fig. 12b and 13a when the same process is undertaken. Therefore, discrete fréchet distances were calculated (using MATLAB) between the 5 % and 25 %, and 25 % and 75 % volumes fraction lines in Fig. 12-a-13a. The ratio of fréchet distances between the 5 % and 25 % line to the 25 % and 75 % line from the RVE response was compared to the ratios obtained from the SPT responses. The results are detailed in the following paragraph.

From the RVE response in Fig. 12a, the fréchet distances are $820x10^6$ (between 5 % and 25 % line) and $1310x10^6$ (between 25 % and 75 %) which correspond to a ratio of 0.626. Similarly, the ratio calculated from Fig. 12b is also 0.626. However, the ratio determined from Fig. 13a has a value of 1 (fréchet distances between 5 % and 25 % line and 25 % and 75 % line are both 20). In addition, considering Fig. 13b the fréchet distances calculated between the lines of yield stress 382.58 MPa and 765.16 MPa and between 765.16 MPa and 1530 MPa are 890 and 1770 respectively.

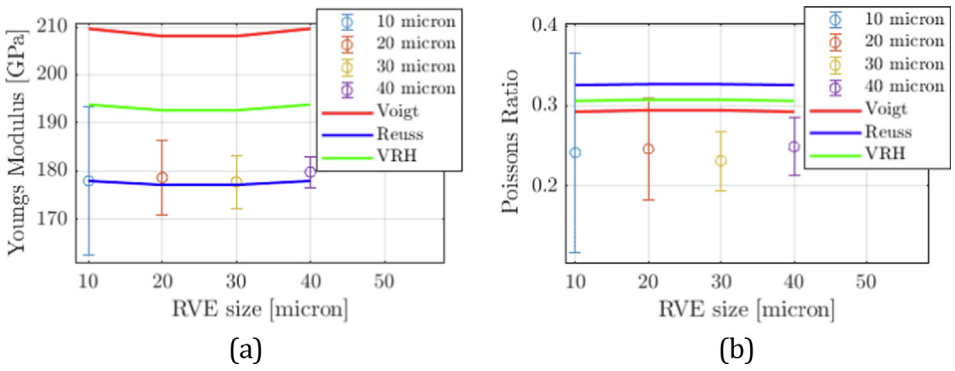

Fig. 8. Diagrams of (a) Young's modulus variation with RVE size plotted against the bounds obtained from the analytical homogenization scheme. And (b) Poisson's ratio variation with RVE size plotted against the bounds obtained from the analytical homogenization scheme.

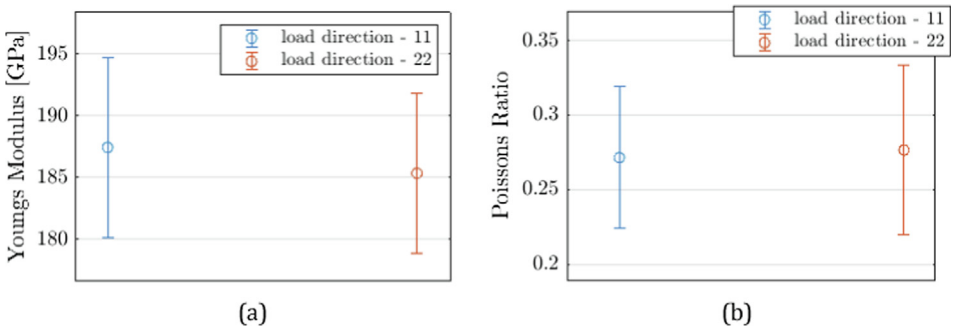

Fig. 9. Plots of (a) Young's modulus variation with loading direction and (b) Pois- son's ratio variation with loading direction.

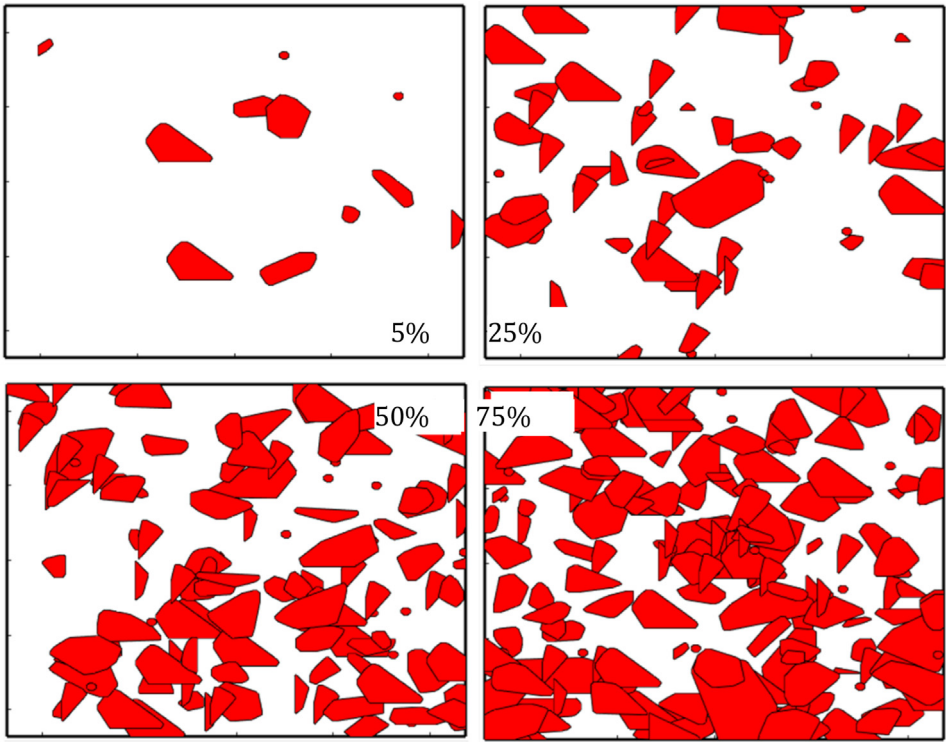

Fig. 10. Plot showing volume fraction of β-phase shown in red. (For interpretation of the references to colour in this figure legend, the reader is referred to the web version of this article.)

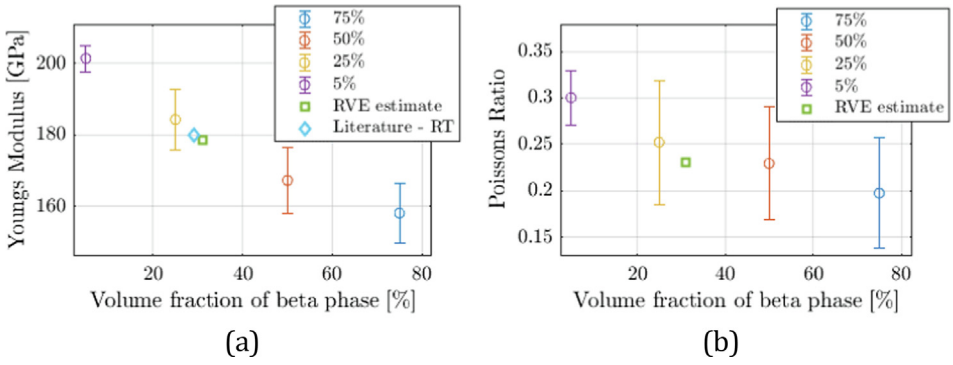

Fig. 11. Plots of impact of β-phase volume fraction on (a) effective Young's Modulus and (b) effective Poisson's Ratio. The'RVE estimate' and'Literature - RT' relate to output obtained from a modelled 40 μm RVE and results obtained from Saeidi's work [30] (at room temperature), respectively.

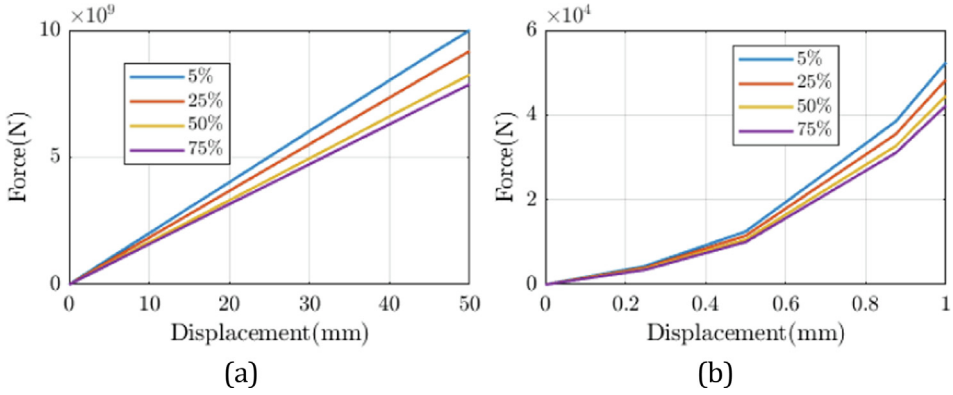

Fig. 12. Diagrams showing force–displacement relationship with changing β-phase fraction for (a) the RVE models and (b) the SPT FE models (without the addition hardening properties).

4. Discussions

From section 3.1, the results of the investigation show that with increasing size of RVE, the spread in effective Young's modulus and Poisson's ratio decreases. For the largest size of RVE of 40 μm simulated in this study, the effective elastic properties are 178.56 ± 7.65 GPa and 0.249 ± 0.037 for Young's modulus and Poisson's Ratio. In Fig. 8a the Young's moduli values show a good level of agreement with the Reuss bound and mean effective Young's moduli for different RVE sizes which lie within 1.12 % of each other. However, from Fig. 8b none of the values of Poisson's ratio are found to be within the bounds determined through the analytical homogenization but the effective Poisson's ratio values lie within 7.23 % of each other. This may be due to an influence of the boundary conditions applied (see Fig. 5a) which may inhibit the free displacement of the edges of the RVE in the transverse direction relative to the load direction, which affects the calculation of Poisson's ratio of the RVE.

The study has also shown an inverse correlation between volume fraction of β- phase and the material effective properties. At 5 % volume fraction Ni is mostly present and the Young's modulus and Poisson's ratio are 200 GPa and 0.3 respectively (see Fig. 11a and 11b). At 31 % β-phase (which is the volume fraction of the bond-coat in the current study) the Young's modulus is 178.56 ± 7.65 GPa (as mentioned previously) and it lies within 0.8 % of the value obtained from literature. This was an expected as a similar result was obtained in an experiment carried by Saeidi et al [30], where the measured Young's modulus of CoNiCrAlY decreased with an increase in volume fraction of β-NiAl phase. Here the volume fraction was varied via heat treatment of the material, where an increased annealing temperature resulted in a reduction in β-phase volume fraction.

Furthermore, from the calculation of fréchet distances and hence their ratios from section 3.3, the ratio obtained from Fig. 12a of 0.626 is the same as that of Fig. 12b. This means that the variation of volume fraction results in a force–displacement response in the RVE that is directly proportional to the response seen by the SPT FE model that has only elastic material properties. However, for the SPT FE model with the yield and hardening implemented in Fig. 13a, the ratio has a value of 1, implying that there are no changes in the SPT results in this model with changing β-phase volume fraction. This suggests that yield and hardening behaviour of the material have more impact on the SPT results than changes in the elastic properties. This is evidenced by the results from Fig. 13b that show that as yield stress was doubled and subsequently halved in SPT FE models, there was proportional change in the response. This was determined through calculating fréchet distances between the lines in the figure and indicates that the SPT may not be applicable to measure variations in mechanical proprieties driven by changes in a material's constituents. Therefore, this has significant implications for scenarios where material design of the bond-coat against de-bonding from the substrate is of concern. This is because the propagation of interfacial cracks between the bond-coat and substrate is driven by the release of stored elastic strain energy[22], through a relaxation of residual stresses in the bond- coat (residual stresses may develop in the bond-coat during the thermally spraying manufacturing process). To design against de-bonding, a thorough understanding of the elastic behaviour of the bond-coat is needed and how this behaviour changes in different operating conditions of the component.

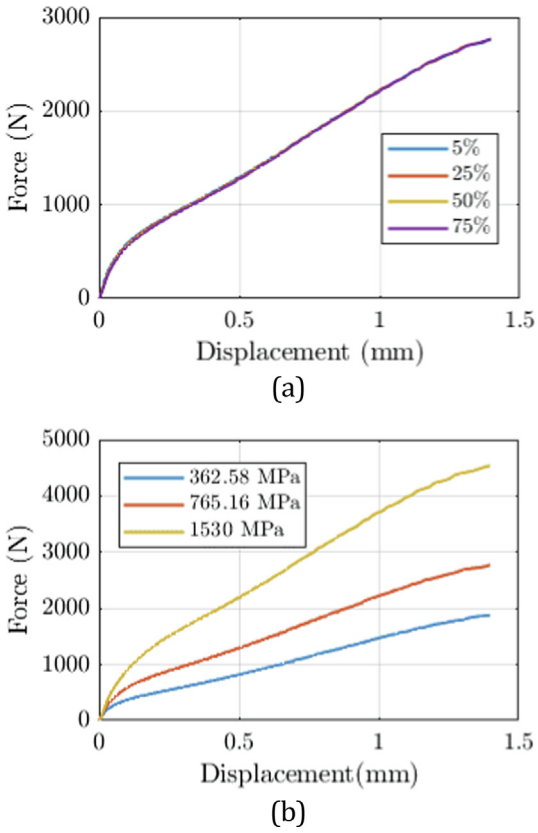

Fig. 13. Plots showing (a) SPT force–displacement results for variation in β phase volume fraction. (b) Force-displacement relationship of SPT for variation in yield stress.

However, the results of this study suggest that using the SPT to determine variations in elastic properties of a specimen material, can be very challenging and that variations in SPT results may point to changes in yield behaviour rather than changes in elastic properties. Furthermore, the elastic regions (see Fig. 2a) in the SPT results shown in Fig. 13a and 13b are relatively small compared to the other regions in the response. Also, a previous study by Chica et al [31] showed that in real SPT experiments, the elastic zone does not just consist of elastic deformation but also includes localized plastic yielding as the punch makes contact with the specimen disc, in the initial stages of the SPT experiments. This understanding along with the findings presented in this study express the challenge in extracting reliable material elastic behavior from the SPT.

5. Conclusions

The main conclusions that can be drawn from this study are:

- Interpretation of elastic behaviour from SPT results is very challenging. The results of this numerical study suggest that the SPT results are insensitive to changes in material elastic behaviour as its results are impacted more by the yield properties of a material.
- The estimates of Young's modulus and Poisson's ratio determined from this study are 178.56 ± 7.65GPa and 0.249 ± 0.037 respectively. These values compare well with those found in literature.
- The value for Young's modulus has a good agreement with the Reuss analytical homogenization scheme and is within 0.8 % of the value obtained from literature. The value of Poisson's ratio however, did not have a good agreement with values obtained from the analytical homogenization scheme. This due to the boundary conditions chosen for the RVE model.
- Lastly, an increase in volume fraction of β-NiAl phase resulted in a decrease in the Young's modulus and Poisson's ratio of CoNiCrAlY. The inverse relationship between volume fraction and effective elastic properties was an expected result and was seen in previous studies.

Data and code availability

The data and code that support the findings of this study are available from the corresponding author upon reasonable request.

Data availability

Data will be made available on request.

Declaration of Competing Interest

The authors declare that they have no known competing financial interests or personal relationships that could have appeared to influence the work reported in this paper.

Appendix A. Supplementary data

Supplementary data to this article can be found online at https://doi.org/10.1016/j.matdes.2023.111601.

References

[1] S. Bose, "Chapter 7 - Thermal Barrier Coatings (TBCs)," in *High Temperature Coatings (Second Edition)* (S. Bose, ed.), pp. 199–299, Butterworth-Heinemann, second edi ed., 2018.
[2] N.P. Padture, M. Gell, E.H. Jordan, Thermal barrier coatings for gas-turbine engine applications, Science 296 (5566) (2002) 280–284.
[3] D.R. Clarke, M. Oechsner, N.P. Padture, Thermal-barrier coatings for more efficient gas-turbine engines, MRS Bulletin 37 (10) (2012) 891–898.
[4] R.J. Lancaster, S.P. Jeffs, B.J. Haigh, N.C. Barnard, Derivation of material properties using small punch and shear punch test methods, Materials and Design 215 (2022) 110473.
[5] G. A. Jackson, W. Sun, and D. G. McCartney, "The influence of microstructure on the ductile to brittle transition and fracture behaviour of HVOF NiCoCrAlY coatings de- termined via small punch tensile testing," *Materials Science and Engineering A*, vol. 754, pp. 479–490, apr 2019.
[6] M. Bruchhausen, S. Holmström, I. Simonovski, T. Austin, J.M. Lapetite, S. Ripplinger, F. De Haan, Recent developments in small punch testing: Tensile properties and DBTT, Theoretical and Applied Fracture Mechanics 86 (2016) 2–10.
[7] H. Chen, T.H. Hyde, K. Voisey, D. Mccartney, Application of small punch creep testing to a thermally sprayed CoNiCrAlY bond coat, Materials Science and Engineering: A 585 (2013) 205–213.
[8] N.P. Padture, M. Gell, E.H. Jordan, Thermal barrier coatings for gas-turbine engine applications, tech. rep. (2002).
[9] F. Cortellino, W. Sun, J. P. Rouse, B. Cacciapuoti, and T. H. Hyde, "Experimental and nu- merical analysis of initial plasticity in P91 steel small punch creep samples," *Experimental Mechanics*, vol. 57, no. 8, 2017.
[10] I. Simonovski, S. Holmström, M. Bruchhausen, Small punch tensile testing of curved specimens: Finite element analysis and experiment, International Journal of Mechanical Sciences 120 (2017) 204–213.
[11] R. Hurst, Y. Li, and K. Turba, "Determination of fracture toughness from the small punch test using circular notched specimens," *Theoretical and Applied Fracture Mechanics*, vol. 103, p. 102238, 2019.
[12] T.E. García, C. Rodríguez, F.J. Belzunce, C. Suárez, Estimation of the mechanical properties of metallic materials by means of the small punch test, Journal of Alloys and Compounds 582 (2014) 708–717.
[13] M. Abendroth, "FEM Analysis of Small Punch Tests," *Key Engineering Materials*, vol. 734, pp. 23–36, 2017.
[14] D. Sánchez-Ávila, A. Orozco-Caballero, E. Martínez, L. Portolés, R. Barea, F. Carreño, High-accuracy compliance correction for nonlinear mechanical testing: Improving Small Punch Test characterization, Nuclear Materials and Energy 26 (October) (2020) 2021.
[15] J. Torres, A.P. Gordon, Mechanics of the small punch test: a review and qualification of additive manufacturing materials, vol. 56, Springer, US, 2021.
[16] "BS EN 10371-2021–[2022-11-11–07-35-36 AM].pdf.".
[17] E. Lucon, "Testing of Small-Sized Specimens," in *Comprehensive Materials Processing*, vol. 1, pp. 135–163, Elsevier Ltd, jan 2014.

[18] H. Chen, G.A. Jackson, W. Sun, An Overview of Using Small Punch Testing for Mechanical Characterization of MCrAlY Bond Coats, Journal of Thermal Spray Technology 26 (2017) 1222–1238.
[19] M. Contreras, C. Rodríguez, F. Belzunce, C. Betegón, The use of small punch test to evaluate the ductile to brittle transition temperature of structural steels, Fatigue & Fracture of Engineering Materials & Structures 31 (2008) 727–737.
[20] W. Wen, G.A. Jackson, H. Li, W. Sun, An experimental and numerical study of a CoNiCrAlY coating using miniature specimen testing techniques, International Journal of Mechanical Sciences 157–158 (2019) 348–356.
[21] J. Nicholls, Designing oxidation-resistant coatings, JOM 52 (2000) 28–35.
[22] P.W. Chen, S.M. Wang, F.H. Wang, Fracture Analysis of Thermal Barrier Coating Delamination under Thermal Shock, Procedia Engineering 99 (2015) 344–348.
[23] J.M.J. den Toonder, J.A.W. van Dommelen, F.P.T. Baaijens, The relation between single crystal elasticity and the effective elastic behaviour of polycrystalline materials: theory, measurement and computation, Modelling and Simulation in Materials Science and Engineering 7 (Nov 1999) 909–928.
[24] G. A. Jackson, M. H. Tsai, P. Mohammadpour, A. Plotkowski, A. Phillion, J. Zhang, Y. Hu, Q. Wei, Y. Xiao, P. Chen, G. Luo, Q. Shen, S. Sheikh, S. Shafeie, Q. Hu, J. Ahlström, C. Persson, J. Veselý, J. Zýka, U. Klement, S. Guo, A. C. Martin, J. P. Oliveira, C. Fink, C. J. Tong, M. R. Chen, S. K. Chen, J. W. Yeh, T. T. Shun, S. J. Lin, S. Y. Chang, G. Skrabalak, A. Stwora, M. L. Grossbeck, J. F. King, D. J. Alexander, P. M. Rice, and G. M. Goodwin, ''In- fluence of microstructure on the mechanical properties of thermally sprayed NiCoCrAlY coatings determined by small punch testing," *Metallurgical and Materials Transactions A: Physical Metallurgy and Materials Science*, vol. 31, no. 2, p. 100936, 2020.
[25] H. Moussaddy, A New Definition of the Representative Volument Element in Numer- ical Homogenization Problems and its Application to the Performance Evaluation of Analytical Homogenization Models, University of Montreal, Thesis, 2013.
[26] J. Segurado, R.A. Lebensohn, J. Llorca, Computational Homogenization of Polycrystals, Advances in Applied Mechanics 51 (April) (2018) 1–114.
[27] G. Frommeyer, R. Rablbauer, H. Schäfer, Elastic properties of b2-ordered nial and nial–x (cr, mo, w) alloys, Intermetallics 18 (3) (2010) 299–305.
[28] J. C. Helton and F. J. Davis, ''Latin hypercube sampling and the propagation of uncertainty in analyses of complex systems," *Reliability Engineering & System Safety*, vol. 81, no. 1, pp. 23–69, 2003.
[29] S.S. Vel, A.C. Cook, S.E. Johnson, C. Gerbi, Computational homogenization and micromechanical analysis of textured polycrystalline materials, Computer Methods in Applied Mechanics and Engineering 310 (2016) 749–779.
[30] S. Saeidi, K. T. Voisey, and D. G. McCartney, ''Mechanical properties and microstructure of VPS and HVOF CoNiCrAlY coatings," *Journal of Thermal Spray Technology*, vol. 20, no. 6, pp. 1231–1243, 2011.
[31] J.C. Chica, P.M. Bravo Díez, M. Preciado Calzada, Improved correlation for elastic modulus prediction of metallic materials in the Small Punch Test, International Journal of Mechanical Sciences 134 (2017) 112–122.